ADVANCED MATERIALS
www.advmat.de

Trap Engineering of CdTe Nanoparticle for High Gain, Fast Response, and Low Noise P3HT:CdTe Nanocomposite Photodetectors

*Haotong Wei, Yanjun Fang, Yongbo Yuan, Liang Shen, and Jinsong Huang**

Highly sensitive photodetectors are needed in wide fields such as defense, industry, health, and scientific research.[1–9] For a high performance photodetector, fast response, high signal-noise ratio, and large linear dynamic range with a proper spectral response band are important in order to meet all the requirements for different applications.[1–4] Photoconductive devices are attractive as highly sensitive photodetectors because of the large gain which is defined as the number of collected charges per absorbed photon. In general, the presence of deep traps in the semiconductor active layer causes a long carrier recombination lifetime for one type of charge, resulting in a high photoconductive gain because the gain is determined by the ratio of recombination lifetime and transit time for the carrier charges to sweep across the device. However, a long charge-trapping lifetime (or recombination lifetime) inevitably leads to a long device response time, which limits their applications. Inorganic nanomaterials including ZnO quantum dots (QDs), PbS QDs, CdS nanobelt, and organic–inorganic hybrid materials, such as organometal trihalide perovskites, have shown excellent photoconductive gain, but the main limit for their application is the low response speed.[3,5–9] For example, PbS QD photodetectors can achieve a high gain with a responsivity of 10^3 A W^{-1} after ligand exchange, which is induced by deep traps of PbS QDs. However, it is difficult to control the trap depth of PbS QDs within a suitable level after synthesis, and eventually leads to a long response time of 70 ms.[5] CdTe nanowires and nanoribbons devices also show long response time of 1 and 3.3 s, respectively, due to the presence of deep traps.[10,11] The charge detrapping lifetime reduces with trap depth since the detrapping is thermally activated. It is thus speculated that removing the deep traps while keep the shallow traps can still maintain the high gain while significantly increases the device response speed. In the recent years, a new family of nanocomposite is synthesized by crafting conjugated polymer on QDs through covalent bond, and the photovoltaic response is improved compared to the simply physical mixture of these two materials.[12–15] The improvement of photovoltaic signal may originate from partial passivation of the traps on the QDs, which should be also promising for photodetector devices. In this work, we prove this hypothesis by studying poly(3-hexylthiophene) (P3HT):CdTe QDs photodetector through trap engineering. By selective passivating deep traps on CdTe QDs surfaces with P3HT, the photodetectors retain a high gain of 50 but have a 25 000 times shorter response time of 2 µs. The high specific detectivity of approaching 10^{13} Jones across the UV–vis range enables the direct detecting weak light intensity of sub 1 pW cm^{-2}.

CdTe QDs were chosen for this study because they have a high light absorption coefficient of over 10^5 cm^{-1} M^{-1} at their first excitonic absorption,[16] and the electrons carrier mobility for CdTe single crystals exceeds 10^3 cm^2 V^{-1} s^{-1}.[17] These properties enable CdTe QDs to be used as a good photoactive layer to absorb light and transport photogenerated charges in a photodetector. CdTe QDs in this study were synthesized according to the literature,[16,18] which were capped with *N*-phenyl-*N′*-methyldithiocarbamate (PMDTC, the corresponding molecular structure can be found in Figure S1a, Supporting Information) after ligand exchange.[19,20] The average diameter of CdTe QDs was about 5.6 nm, which was calculated from the exciton absorption peak (Figure S1b, Supporting Information). The energy diagram of PMDTC-capped CdTe QDs is shown in **Figure 1**a. Electrons are confined in the core of CdTe crystal due to the energy band offset between conduction band minimal (CBM) with the lowest unoccupied molecular orbital (LUMO) of PMDTC, while photogenerated holes are transferred to the PMDTC. Therefore, CdTe QDs act as electron-traps. For CdTe bulk materials, the reported defects causing electron-traps are Te vacancy V_{Te}^{2+}, antisite Cd_{Te} and Cd interstitials Cd_i^{2+}.[21] Among them V_{Te}^{2+} and Cd_{Te} cause shallow electron-traps with a trap depth of 0.04–0.06 eV below CBM, while Cd_i^{2+} causes deep electron-traps with a large trap depth of 0.64 eV. For CdTe QDs, due to the incomplete coverage of ligand, Cd^{2+} is rich in the QDs surface. It has been reported that different oxide species on surface of QDs result in different trap states,[22] and more oxygen contained species have longer trapping lifetime, which are often recognized as deep traps. PbS QDs films with species of $PbSO_4$, $PbSO_3$, and Pb-carboxylate have photocurrent decay time of 2 s, 300 ms, and 60 ms, respectively.[22] Cd^{2+} may also form different oxide species which act as deep traps and cause a long decay time. In order to passivate these deep traps, we employed P3HT to engineer the traps of CdTe QDs. Here P3HT and CdTe QDs blended solution was spinning-coated onto hole transport layer covered indium tin oxide (ITO) glass to make nanocomposite films, and the films were solvent annealed in 1,2-Dichlorobenzene (DCB) atmosphere for 8 h. The principle of engineering CdTe deep traps by P3HT is illustrated in

Dr. H. Wei, Dr. Y. Fang, Dr. Y. Yuan, Dr. L. Shen, Prof. J. Huang
Department of Mechanical and Materials Engineering
University of Nebraska-Lincoln
Lincoln, NE 68588, USA
E-mail: jhuang2@unl.edu

DOI: 10.1002/adma.201502292

© 2015 WILEY-VCH Verlag GmbH & Co. KGaA, Weinheim

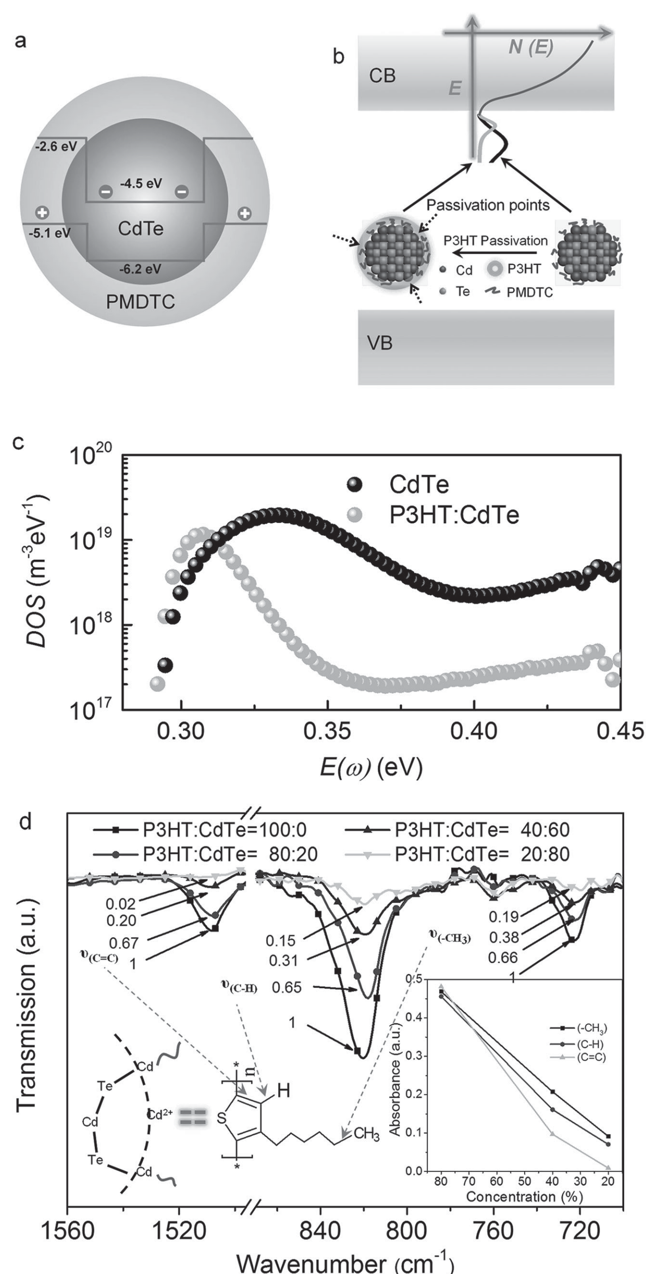

Figure 1. a) The scheme of electron-trap process of PMDTC-capped CdTe QDs. b) The QDs passivation process scheme. Uncovered Cd^{2+} trap points are coordinated with P3HT molecular, and the deep electron-traps states are significantly eliminated. c) The trap density of state for CdTe and P3HT:CdTe electron-only devices under –0.5 V bias. d) FTIR spectra of P3HT:CdTe films with different P3HT contents, and the 722, 818, 1508 cm^{-1} signal peaks from P3HT are labeled. The inset figure shows the absorption changes of the three peaks with P3HT loading ratio.

Figure 1b. Since the deep traps are most likely caused by the oxidized Cd^{2+} species, we hypothesize that the Cd^{2+} on the CdTe QDs can be passivated by S atoms of P3HT through forming Cd–S coordination bonds, so that Cd^{2+} can no longer form oxide species. Through S atoms coordination interaction, surface Cd^{2+} related deep traps can be selectively passivated, while the shallow traps such as V_{Te}^{2+}, Cd_{Te} and the trap due to energy offset of CdTe and ligand can be maintained.

To verify the passivation of deep electron-traps, we measured the energy dependent trap density distribution of the nanocomposite material using thermal admittance spectroscopy method.[23] For this measurement, electron-only devices were fabricated so that only electron-traps were measured with structure of ITO/Cs_2CO_3/CdTe or P3HT:CdTe/Cs_2CO_3/Al. The trap density of states verses demarcation energy curves of the electron-only CdTe and P3HT:CdTe nanocomposite devices are shown in Figure 1c.[24,25] It can be seen that the electron-trap density state of P3HT:CdTe device was significantly lower than that of CdTe device at high demarcation energy (0.37–0.45 eV), while the electron-trap density states of the two devices were similar at low demarcation energy (≈0.31 eV). It indicates that the deep trap states on CdTe surface can be selectively passivated by P3HT while the shallow trap states remain, which is in accordance with our assumption. We assign the shallow traps of 0.31 eV to the confinement of electrons in CdTe core by the ligand.

Fourier transform infrared spectroscopy (FTIR) measurement was performed to verify the formation of Cd–S coordination bonds, and the results are shown in Figure 1d. It is unfortunately not feasible to directly determine the Cd–S bond formation by monitoring the Cd–S bond vibration, because S also presents in the ligand. Here, we monitored the change vibration intensity of other chemical bonds on P3HT, because they should be reduced if S atoms on P3HT is fixed to CdTe QDs. Nevertheless, the degree of reduction is expected to be different, depending on the distance of this chemical bond with the Cd–S bond. We identified three major vibrations peaks at 1508, 818, and 722 cm^{-1}, which correspond to C=C stretching vibration, aromatic C–H bond out of plane vibration, and C–H vibration in the methyl rock, respectively. Since the C=C bond is closest to the Cd–S bond, its vibration intensity should be strongest affected. For the same token, the C–H vibration in the methyl rock should be least affected due to its largest distance with Cd–S bond. Four P3HT:CdTe samples with different P3HT loading ratio were measured, and the spectra were normalized by the 1258 cm^{-1} peak which corresponded to the C–N bond on CdTe surface in order to exclude the influence of different amount of CdTe QDs in each sample. We can see that the absorption peak intensity of all these three peaks decreased as the percentage of P3HT in the nanocomposite materials decreased.[26] However, the decreasing rates were different as summarized by the inset of Figure 1d. The absorbance of methyl rock peak had a linear relationship with P3HT percentage, while the absorbance peaks of the C=C and aromatic C–H bonds decreased faster than the P3HT concentration change. The decreasing rate of the absorbance for C=C bond vibration was the fastest. This is fully agreement with our speculation, and thus confirms the formation of Cd–S coordination bonds after mixing P3HT and CdTe QDs. It is noted that C=C stretching vibration signal disappeared when P3HT loading ratio is reduced to 20%, which indicates that most S atoms on P3HT formed Cd–S bond with Cd^{2+} on CdTe QDs surface.[26] Moreover, the coordination efficiency is over 90% according to the ratio of decreased peak intensity of C=C bond when the P3HT content is 20%. Therefore, the passivation of

© 2015 WILEY-VCH Verlag GmbH & Co. KGaA, Weinheim
Adv. Mater. 2015,
DOI: 10.1002/adma.201502292

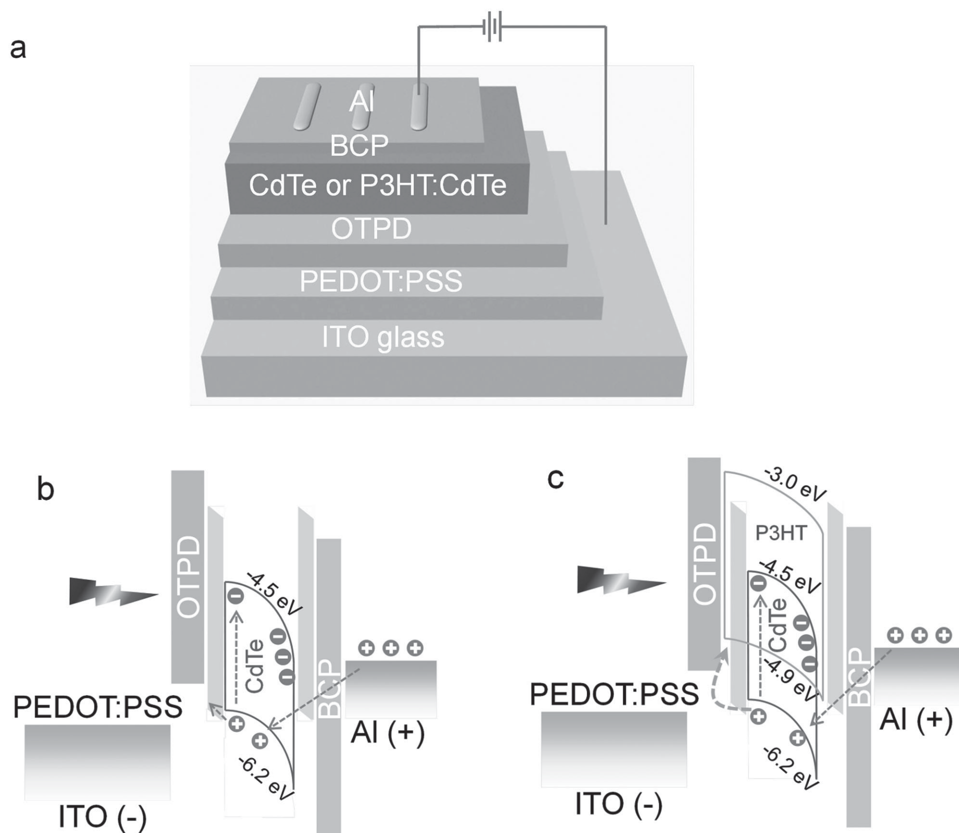

Figure 2. a) The device structure of CdTe and P3HT:CdTe nanocomposite photodetectors. b,c) The energy band structures of the CdTe and P3HT:CdTe devices under illumination and under an applied reverse bias.

CdTe QDs by P3HT should originate from eliminating deep traps caused by Cd^{2+} related oxide species, because capping CdTe QDs by P3HT coordination bonds prevents the oxidation of Cd^{2+}. The wrapping effect of CdTe QDs by P3HT is characterized by atomic force microscope (AFM) as shown in Figure S2, Supporting Information. The phase image of P3HT:CdTe film is more uniform than that of CdTe QDs film because the exposed CdTe surface area is decreased by P3HT wrapping.

Photodetectors with two kinds of active layers of CdTe QDs or P3HT:CdTe QDs were fabricated to find out the passivation effect of CdTe QDs deep traps on device performance. Vertical device structure was employed so that the transit distance and the transit time of carriers can be minimized (**Figure 2**a). Poly(3,4-ethylenedioxythiophene):poly(styrenesulfonate) (PEDOT:PSS) and N4,N4′-bis(4-(6-((3-ethyloxetan-3-yl)methoxy)hexyl)phenyl)-N4,N4′-diphenylbiphenyl-4,4′-diamine (OTPD) were employed as holes-transporting/electrons-blocking layer, and 2,9-dimethyl-4,7-diphenyl-1,10-phenanthroline (BCP) layer was used as electrons-transporting/holes-blocking layer. For the OTPD layer formation, UV cross-linking process was performed to prevent this layer from being washed away by the following spin-coating process.

The energy band structures of the CdTe device and the P3HT:CdTe device are presented in Figure 2b,c, respectively. Trapped electrons in CdTe QDs act as the space charges to cause band-bending in the CdTe films and the P3HT:CdTe blended films, which significantly reduces hole injection barrier. Under illumination, holes can be easily injected into the active layer from Al electrode even under a small reverse bias, which enables a large photoconductive gain in these devices. External quantum efficiency (EQE) measurement was conducted at different reverse biases to characterize the device photoconductive gain directly. As shown in **Figure 3**a, the EQE value of the CdTe device exceeded 100% at −3 V bias, and increased rapidly with the bias. The peak EQE value of the CdTe device at 390 nm reached 4300% at −6.4 V. An obvious increase of reverse-bias photocurrent was observed, which is in good correspondence to the EQE change (Figure 3b). The EQE value can be above 100%, because in addition to the photogenerated charges, charges flowing through the external circuit also include injected ones from the electrodes under an applied bias, and this part of charges can be only injected under illumination because of the large energy barrier prevents the charge injection in the dark. The number of injected charges can be significantly higher than that of the photogenerated charges, so the resulting gain can be much larger than 1 (or EQE of 100%). The multiple exciton generation effect and avalanche effect should be excluded for the mechanism of the observed large gain because of the too small bias and very large gain observed here. Introducing P3HT into the CdTe films did not reduce the EQE (Figure 3c), while reduced the dark current density (J_d) significantly. Usually, eliminating the deep traps of a device

© 2015 WILEY-VCH Verlag GmbH & Co. KGaA, Weinheim

COMMUNICATION

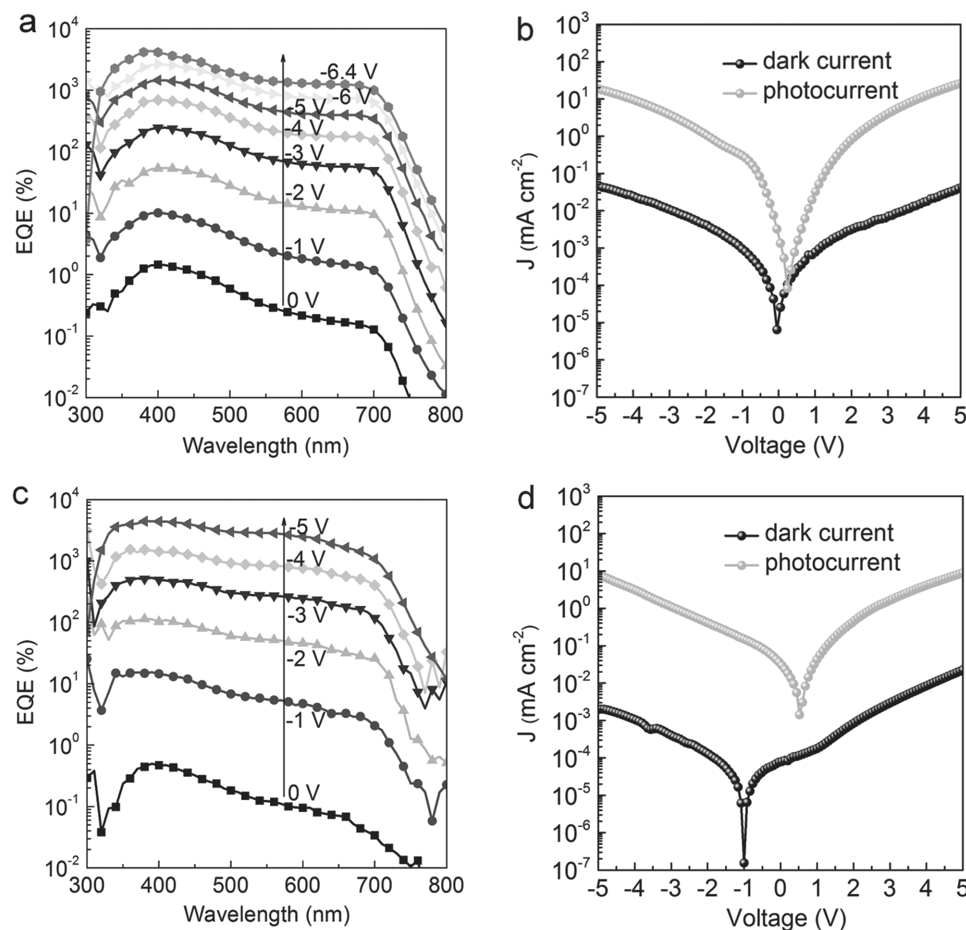

Figure 3. a,c) The EQE spectra at different reverse bias for the CdTe and P3HT:CdTe device. b,d) The *J*–*V* curves in the dark and under illumination for the CdTe and the P3HT:CdTe devices.

may decrease the gain due to the shorten charge recombination time, however, the P3HT:CdTe device almost had the same gain with the CdTe device after trap engineering by P3HT. This is because the holes mobility of P3HT is much higher than that of PMDTC (Figure S3, Supporting Information), so holes are mainly transported by P3HT in the P3HT:CdTe device, which contributes to a shorter transit time, and eventually leads to a similar gain. For the CdTe QDs device, the J_d was ≈50 μA cm^{-2} at –5 V, while the J_d of P3HT:CdTe device was only 1.9 μA cm^{-2} at –5 V, as shown in Figure 3d. The large J_d of CdTe device may be due to the incomplete coverage of ligands on CdTe QDs or pin–holes leakage due to the noncompact nanoparticle films. This can explain the high EQE value of over 8000% for CdTe device without BCP layer (Figure S4, Supporting Information). After introducing P3HT into CdTe QDs, CdTe QDs were capped and well dispersed in the P3HT matrix, which can significantly decrease the leakage. In addition, passivate the deep electron-traps did not change the dominant trap type (electron-trap device), because the electron-trap density was still higher than the hole-trap density (Figure S5, Supporting Information), which enabled that our device was still a hole dominated device.

A shorter transit time and trapping time in the P3HT:CdTe device should result in a short response time after passivating the deep traps. The response time was measured, and the transient photocurrent was generated by a chopper modulated 532 nm laser pulse, and recorded by an oscilloscope. As shown in **Figure 4**a, the response time of CdTe device was >50 ms. On the other hand, the response time of P3HT:CdTe device was much shorter. Since the response speed was so fast that the slow chopper rotation rate already limited the measurement (Figure 4b), we used a 337 nm laser pulse with a pulse width of 4 ns to accurately measure the response time. As shown in Figure 4c, the decay of photocurrent consisted of a fast process of 0.2 μs and a slow process of 1.6 μs. This response speed was among the highest reported value among all nanoparticles or QDs based photodetectors.[3,5–9] The fast response speed in P3HT:CdTe device further proves that Cd^{2+} related deep traps are all passivated by P3HT. The transit time of the P3HT:CdTe device was calculated to be 73 ns using the hole mobility of 1.1×10^{-3} cm^2 V^{-1} s^{-1} derived from space charge-limited-current (SCLC) method (Figure S3a, Supporting Information). Photoconductive gain was calculated to be about 28 using the ratio of recombination time and transit time, which was smaller but close to the gain measured by EQE. While the transit time of CdTe device was calculated to be 47 μs, which is much longer than that of P3HT:CdTe

© 2015 WILEY-VCH Verlag GmbH & Co. KGaA, Weinheim
Adv. Mater. **2015**,
DOI: 10.1002/adma.201502292

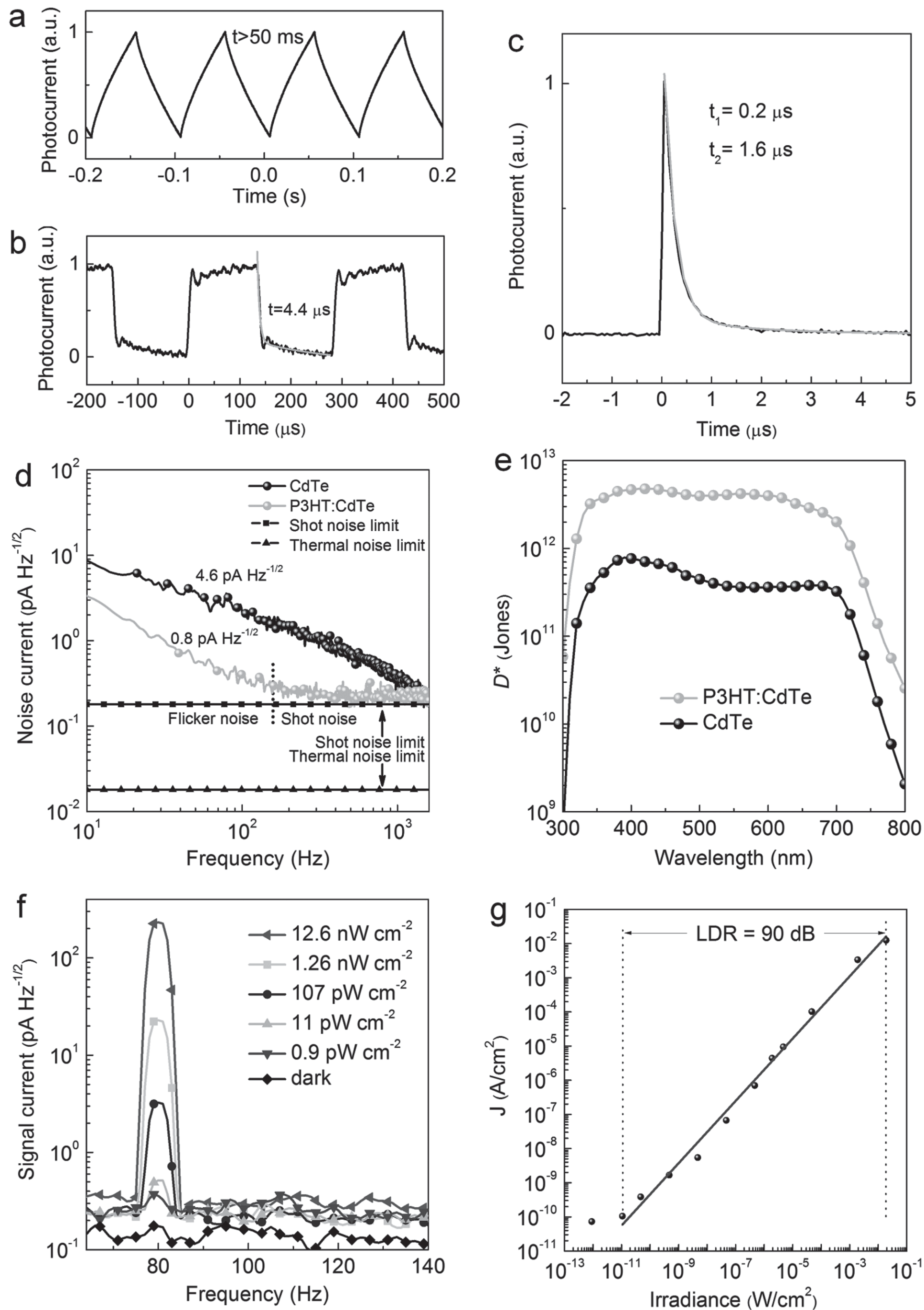

Figure 4. The transient photocurrent of the a) CdTe device and b) the P3HT:CdTe device measured under a bias of −5 V with an optical chopper controlled 532 nm laser pulses. c) The transient photocurrent decay curve of the P3HT:CdTe device excited by a 337 nm laser pulse. d) The noise current of the CdTe and the P3HT:CdTe devices under −5 V bias. e) The specific detectivity of CdTe and P3HT:CdTe devices under −5 V bias. f) The measured signal current of the P3HT:CdTe nanocomposite photodetector by a FFT spectrum analyzer under changed light intensity to distinguish the weakest detectable light intensity from noise. g) Linear dynamic range measurement result of the P3HT:CdTe photodetector.

device due to low holes carrier mobility of PMDTC ligand (Figure S3b, Supporting Information).

The figure of merit of a photodetector is the specific detectivity (D^*) which characterizes the capability of a photodetector to detect the weakest light signal.[9] In addition to the responsivity, the other important factor that influences the specific detectivity is the noise current. Usually, a low dark current predicts a low noise current. If the noise is mainly dominated by shot noise, it can be directly calculated from the dark current. However, in many instances, charge traps in the photoactive layer may change the origin of noise. Frequency dependent flicker noise due to the trapping-detrapping of charge carriers

© 2015 WILEY-VCH Verlag GmbH & Co. KGaA, Weinheim

is commonly encountered, and it is often much larger than the shot noise.[9] Therefore, it is more accurate to measure the noise current instead of calculating it from dark current. We believe that passivating the deep trap of CdTe QDs by P3HT should reduce the device noise current, and the noise type may change from flicker noise to shot noise because the charge trapping and detrapping process is reduced. Figure 4d shows the directly measured noise current of the CdTe and P3HT:CdTe devices at different frequency by a fast Fourier transform (FFT) signal analyzer which was connected to a low noise current preamplifier. It can be clearly seen that the noise current of the P3HT:CdTe device was about one order of magnitude lower than that of the CdTe device at −5 V bias below 200 Hz. The noise of the CdTe device was completely dominated by 1/f noise, while the noise of the P3HT:CdTe device was dominated by shot noise for >160 Hz. The noise current of P3HT:CdTe device at 35 Hz was only 0.8 pA $Hz^{-1/2}$. P3HT:CdTe device presents low noise and high responsivity through engineering the trap depth of CdTe, which can result in a high specific detectivity according to Equations (1) and (2)[3]

$$D^* = \frac{(AB)^{1/2}}{NEP}\ (\text{cm Hz}^{1/2}\ \text{W}^{-1}\ \text{or Jones}) \quad (1)$$

$$NEP = \frac{\overline{i^2}^{1/2}}{R}\ (\text{WHz}^{-1/2}) = \frac{\overline{i^2}^{1/2}}{q \cdot EQE / h\nu}\ (\text{WHz}^{-1/2}) \quad (2)$$

where A is the device area, B is the bandwidth, NEP is the noise equivalent power, $\overline{i^2}^{1/2}$ is the measured noise current, R is the responsivity, h is the Planck constant, ν is the frequency of light. The peak responsivity of the P3HT:CdTe photodetector at 380 nm was 13.6 A W^{-1}, and the corresponding D^* was about 4.5×10^{12} Jones as plotted in Figure 4e. D^* of P3HT:CdTe device was about five times higher than that of CdTe device, and it remained approaching 10^{13} Jones from 300 to 700 nm.

A high specific detectivity means that the device can detect weak light. Based on the noise current of 8×10^{-13} A $Hz^{-1/2}$ at 35 Hz, the responsivity of 10.8 A W^{-1} at 350 nm, the NEP was calculated to be 7.4×10^{-14} W $Hz^{-1/2}$ according to Equation (2). It means that our photodetector can distinguish the weakest light intensity of 1 pW cm^{-2} from noise considering its working area of 7 mm^2. This estimation stands only if the device responsivity keeps constant under a weak light intensity down to the NEP level, because the responsivity is derived under strong illumination. Therefore, it is necessary to directly characterize the NEP of our photodetector to confirm the large calculated detectivity. Here the total current of the photodetector at different light intensity under the reverse bias of −5 V was recorded by a FFT spectrum analyzer in the same way as noise current measurement. A 350 nm emission light LED was modulated to be 80 Hz frequency by a function generator, and the light intensity was severely attenuated by neutral density filters from 12.6 nW cm^{-2} to 0.9 pW cm^{-2}. As shown in Figure 4f, there was a photocurrent signal peak at 80 Hz when the light intensity was about 12.6 nW cm^{-2}, and the photocurrent signal was proportional to the light intensity as the intensity change. When the light intensity was low enough, the signal can be no longer distinguished from the noise current, and that light intensity should be the NEP of the photodetector. It can be seen that the lowest detectable light intensity for our device was about 0.9 pW cm^{-2}, and it was close to the NEP calculation result. Benefited from the reduced noise, this kind of nanocomposite photodetector also had a wide linear dynamic range (LDR). From Figure 4g we can see that the device photocurrent exhibited a linear relationship within the light intensity range from 0.019 W cm^{-2} to about 10 pW cm^{-2}. The LDR was more than 90 dB, which was significantly larger than that of the InGaAs detector (66 dB) and GaN detector (50 dB).[2,27] These photodetectors had a stable photocurrent output at work condition (−5 V) under white light illumination with intensity of 100 mW cm^{-2} (Figure S6, Supporting Information). There was little degradation of photocurrent after over 35 min continuous measurement.

In conclusion, we fabricated P3HT:CdTe QDs nanocomposite photodetectors and proposed a strategy of tailoring the trap depth of CdTe QDs device by trap engineering. Cd^{2+} related deep traps on CdTe QDs surface were selectively passivated by P3HT coordination, while the shallow traps can still trigger a high gain of 50 as well as a short response time of 2 µs. The noise of the P3HT:CdTe device was significantly reduced compared to that of the device without trap passivation, resulting in a high specific detectivity of approaching 10^{13} Jones. The NEP of our photodetectors was directly measured to prove that it could detect a weak light intensity of 0.9 pW cm^{-2}. The nanocomposite device also had a large LDR of over 90 dB. The excellent combination of gain, response speed, sensitivity, LDR, and stability of P3HT:CdTe QDs photodetectors paved the way for a wide range of applications in different fields.

Supporting Information

Supporting Information is available from the Wiley Online Library or from the author.

Acknowledgements

This work was financially supported by the Defense Threat Reduction Agency (Award No. HDTRA1–14–1–0030).

Received: May 13, 2015
Revised: June 14, 2015
Published online:

[1] V. Sukhovatkin, S. Hinds, L. Brzozowski, E. H. Sargent, *Science* **2009**, *324*, 1542.
[2] X. Gong, M. Tong, Y. Xia, W. Cai, J. S. Moon, Y. Cao, G. Yu, C. L. Shieh, B. Nilsson, A. J. Heeger, *Science* **2009**, *325*, 1665.
[3] F. Guo, B. Yang, Y. Yuan, Z. Xiao, Q. Dong, Y. Bi, J. Huang, *Nat. Nanotechnol.* **2012**, *7*, 798.
[4] J. W. Lee, D. Y. Kim, F. So, *Adv. Funct. Mater.* **2015**, *25*, 1233.
[5] G. Konstantatos, I. Howard, A. Fischer, S. Hoogland, J. Clifford, E. Klem, L. Levina, E. H. Sargent, *Nature* **2006**, *442*, 180.
[6] S. A. McDonald, G. Konstantatos, S. Zhang, P. W. Cyr, E. J. Klem, L. Levina, E. H. Sargent, *Nat. Mater.* **2005**, *4*, 138.
[7] K. Deng, L. Li, *Adv. Mater.* **2014**, *26*, 2619.

© 2015 WILEY-VCH Verlag GmbH & Co. KGaA, Weinheim

DOI: 10.1002/adma.201502292

[8] L. Dou, Y. M. Yang, J. You, Z. Hong, W. H. Chang, G. Li, Y. Yang, *Nat. Commun.* **2014**, *5*, 5404.
[9] R. Dong, Y. Fang, J. Chae, J. Dai, Z. Xiao, Q. Dong, Y. Yuan, A. Centrone, X. C. Zeng, J. Huang, *Adv. Mater.* **2015**, *27*, 1912.
[10] X. Xie, S. Y. Kwok, Z. Lu, Y. Liu, Y. Cao, L. Luo, J. A. Zapien, I. Bello, C. S. Lee, S. T. Lee, W. Zhang, *Nanoscale* **2012**, *4*, 2914.
[11] M. Shaygan, K. Davami, N. Kheirabi, C. K. Baek, G. Cuniberti, M. Meyyappan, J. S. Lee, *Phys. Chem. Chem. Phys.* **2014**, *16*, 22687.
[12] M. He, F. Qiu, Z. Lin, *J. Phys. Chem. Lett.* **2013**, *4*, 1788.
[13] J. Xu, J. Wang, M. Mitchell, P. Mukherjee, M. Jeffries-El, J. W. Petrich, Z. Lin, *J. Am. Chem. Soc.* **2007**, *129*, 12828.
[14] L. Zhao, X. Pang, R. Adhikary, J. W. Petrich, M. Jeffries-El, Z. Lin, *Adv. Mater.* **2011**, *23*, 2844.
[15] L. Zhao, X. Pang, R. Adhikary, J. W. Petrich, Z. Lin, *Angew. Chem. Int. Ed.* **2011**, *50*, 3958.
[16] W. W. Yu, L. Qu, W. Guo, X. Peng, *Chem. Mater.* **2003**, *15*, 2854.
[17] K. Suzuki, S. Seto, T. Sawada, K. Imai, *IEEE Trans. Nucl. Sci.* **2002**, *49*, 1287.
[18] W. W. Yu, Y. A. Wang, X. Peng, *Chem. Mater.* **2003**, *15*, 4300.
[19] H. Y. Chen, M. K. Lo, G. Yang, H. G. Monbouquette, Y. Yang, *Nat. Nanotechnol.* **2008**, *3*, 543.
[20] Y. Zhao, W. Pérez-Segarra, Q. Shi, A. Wei, *J. Am. Chem. Soc.* **2005**, *127*, 7328.
[21] X. Mathew, *Sol. Energy Mater. Sol. C.* **2003**, *76*, 225.
[22] G. Konstantatos, L. Levina, A. Fischer, E. H. Sargent, *Nano Lett.* **2008**, *8*, 1446.
[23] Y. Fang, F. Guo, Z. Xiao, J. Huang, *Adv. Opt. Mater.* **2014**, *2*, 348.
[24] J. A. Carr, S. Chaudhary, *J. Appl. Phys.* **2013**, *114*.
[25] J. A. Carr, S. Chaudhary, *Energy Environ. Sci.* **2013**, *6*, 3414.
[26] H.-C. Liao, S.-Y. Chen, D.-M. Liu, *Macromolecules* **2009**, *42*, 6558.
[27] M. A. Khan, J. N. Kuznia, D. T. Olson, J. M. Van Hove, M. Blasingame, L. F. Reitz, *Appl. Phys. Lett.* **1992**, *60*, 2917.

© 2015 WILEY-VCH Verlag GmbH & Co. KGaA, Weinheim